

Available online at www.sciencedirect.com

SciVerse ScienceDirect

journal homepage: www.elsevier.com/locate/watres

Transport and retention of multi-walled carbon nanotubes in saturated porous media: Effects of input concentration and grain size

Daniela Kasel^{a,*}, Scott A. Bradford^b, Jiří Šimůnek^c, Marc Heggen^{d,e}, Harry Vereecken^a, Erwin Klumpp^a

^aAgrosphere Institute (IBG-3), Forschungszentrum Jülich GmbH, 52425 Jülich, Germany

^bUS Salinity Laboratory, Agricultural Research Service, United States Department of Agriculture, Riverside, CA 92507, USA

^cDepartment of Environmental Sciences, University of California Riverside, Riverside, CA 92521, USA

^dPeter Grünberg Institute (PGI-5), Forschungszentrum Jülich GmbH, 52425 Jülich, Germany

^eErnst Ruska-Centre (ER-C), Forschungszentrum Jülich GmbH, 52425 Jülich, Germany

ARTICLE INFO

Article history:

Received 1 August 2012

Received in revised form

9 November 2012

Accepted 13 November 2012

Available online 23 November 2012

Keywords:

Carbon nanotubes

Column experiments

Quartz sand

Breakthrough curves

Retention profiles

Transport modeling

ABSTRACT

Water-saturated column experiments were conducted to investigate the effect of input concentration (C_0) and sand grain size on the transport and retention of low concentrations (1, 0.01, and 0.005 mg L⁻¹) of functionalized ¹⁴C-labeled multi-walled carbon nanotubes (MWCNT) under repulsive electrostatic conditions that were unfavorable for attachment. The breakthrough curves (BTCs) for MWCNT typically did not reach a plateau, but had an asymmetric shape that slowly increased during breakthrough. The retention profiles (RPs) were not exponential with distance, but rather exhibited a hyper-exponential shape with greater retention near the column inlet. The collected BTCs and RPs were simulated using a numerical model that accounted for both time- and depth-dependent blocking functions on the retention coefficient. For a given C_0 , the depth-dependent retention coefficient and the maximum solid phase concentration of MWCNT were both found to increase with decreasing grain size. These trends reflect greater MWCNT retention rates and a greater number of retention locations in the finer textured sand. The fraction of the injected MWCNT mass that was recovered in the effluent increased and the RPs became less hyper-exponential in shape with higher C_0 due to enhanced blocking/filling of retention locations. This concentration dependency of MWCNT transport increased with smaller grain size because of the effect of pore structure and MWCNT shape on MWCNT retention. In particular, MWCNT have a high aspect ratio and we hypothesize that solid phase MWCNT may create a porous network with enhanced ability to retain particles in smaller grain sized sand, especially at higher C_0 . Results demonstrate that model simulations of MWCNT transport and fate need to accurately account for observed behavior of both BTCs and RPs.

© 2012 Elsevier Ltd. All rights reserved.

* Corresponding author. Tel.: +49 2461 61 3521; fax: +49 2461 61 2518.

E-mail addresses: d.kasel@fz-juelich.de (D. Kasel), scott.bradford@ars.usda.gov (S.A. Bradford), jiri.simunek@ucr.edu (J. Šimůnek), m.heggen@fz-juelich.de (M. Heggen), h.vereecken@fz-juelich.de (H. Vereecken), e.klumpp@fz-juelich.de (E. Klumpp).

0043-1354/\$ – see front matter © 2012 Elsevier Ltd. All rights reserved.

<http://dx.doi.org/10.1016/j.watres.2012.11.019>

1. Introduction

Carbon nanotubes (CNT) are needle-shaped particles with nano-scale diameters and micro-scale lengths (Iijima, 1991; Mauter and Elimelech, 2008). In principle, CNT are rolled up sheets of graphene forming individual tubes (single-walled carbon nanotubes, SWCNT) or tubes within tubes (multi-walled carbon nanotubes, MWCNT) (Sinnott, 2002). Carbon nanotubes exhibit unique electronic, chemical, and physical properties that have been exploited in numerous commercial applications (Liu et al., 2009; Mattison et al., 2011). The widespread use and a lack of regulations for CNT disposal will undoubtedly result in their release into the environment, especially into soils and groundwater (Nowack and Bucheli, 2007; Klaine et al., 2008; Köhler et al., 2008; Jaisi and Elimelech, 2009). However, the fate and effects of CNT in the environment are still not yet well understood (Saleh et al., 2008). Previous studies have revealed a potential health risk of CNT to several organisms, e.g., rainbow trout and rats (Lam et al., 2006; Handy et al., 2008; Farré et al., 2009). Furthermore, CNT are one of the most biologically non-degradable man-made materials (Lam et al., 2004). The transport of CNT through porous media is therefore of considerable interest regarding potential risks to organisms and human health (Mattison et al., 2011). This is especially true for CNT that have been functionalized to increase their stability in aqueous suspensions because this modification will also increase their mobility in the environment (Mattison et al., 2011).

To date, several studies have investigated CNT transport in packed sand columns under water-saturated conditions. The transport and retention of CNT has been found to be sensitive to a diversity of experimental conditions including ionic strength (IS), pore water velocity, and collector grain size (Jaisi et al., 2008; Jaisi and Elimelech, 2009; Liu et al., 2009; Tian et al., 2010; Mattison et al., 2011; Tian et al., 2012). Despite this research, transport and retention processes for MWCNT are still not completely understood (Mattison et al., 2011). For example, the effect of CNT input concentration on their transport behavior has not yet been reported, and the selected input CNT concentrations for previous studies were more than nine orders of magnitude higher than is expected for most environmentally relevant scenarios (Gottschalk et al., 2009). This is an important aspect to consider because the input concentration has been demonstrated to significantly influence colloid deposition (Bradford and Bettahar, 2006; Bradford et al., 2009), and this concentration effect was also found to depend on the grain size (Bradford and Bettahar, 2006). In general, transport studies at low CNT concentrations are of interest for fundamental research but recent studies only considered input concentration significantly higher than 1 mg L^{-1} (Jaisi et al., 2008; Jaisi and Elimelech, 2009; Liu et al., 2009; Tian et al., 2010; Mattison et al., 2011; Tian et al., 2012). Environmental concentrations of MWCNT will depend on their source and on hydro-geochemical conditions. However, initial model estimates predict very low CNT concentrations in soils in the range of several ng kg^{-1} (Mueller and Nowack, 2008; Gottschalk et al., 2009). In addition, information on retention profiles for CNT is very scarce (Wang et al., 2012b). Retention profiles provide needed

information for mass balance and useful insight on controlling mechanisms of retention (Bradford and Bettahar, 2005). Furthermore, breakthrough curves and retention profiles need to both be accurately simulated by numerical models in order to reliably predict environmental fate and risk (Bradford et al., 2003).

The aim of this study was to investigate the transport and retention of MWCNT in saturated porous media for different input concentrations and sand grain sizes. Three sand grain sizes (607, 350, and $240 \mu\text{m}$) were considered in these studies. The input MWCNT concentrations were 1, 0.01, and 0.005 mg L^{-1} . In addition to breakthrough curves, retention profiles were measured and numerically modeled in order to obtain information on MWCNT mass balance, retention mechanisms, and to more accurately predict environmental fate.

2. Materials and methods

2.1. Carbon nanotubes

Radioactively (^{14}C) labeled MWCNT were prepared by catalytic chemical vapor deposition (Bayer Technology Services GmbH, 51368 Leverkusen, Germany) using ^{14}C -benzene as feedstock gas. The synthesis procedure was a lab-scale setup of the Baytubes[®] production process with slight modifications (Bierdel et al., 2007). After synthesis, the MWCNT were boiled in 70% nitric acid (Sigma–Aldrich Chemie GmbH, 89555 Steinheim, Germany) for 4 h under reflux to remove residual metal catalysts and to enhance their stability in the aqueous phase by addition of oxygen containing functional groups (e.g. carboxylic groups) to their surfaces (Nagasawa et al., 2000; Pumera, 2007; Xia et al., 2007; Smith et al., 2009). Afterwards, the MWCNT were removed from the acid by filtering through a $0.45 \mu\text{m}$ polytetrafluoroethylene (PTFE) membrane and rinsing with deionized water until a neutral pH-value was achieved in the filtrate (Mattison et al., 2011). Finally, functionalized MWCNT were dried in an oven at $45 \text{ }^\circ\text{C}$ and stored at room temperature until needed.

Morphological properties of MWCNT were characterized using a transmission electron microscope (TEM, Philips CM20 FEG, FEI Company, 5651 GG Eindhoven, The Netherlands). The amount of metal catalysts before and after the acid treatment was determined using inductively coupled plasma-mass spectrometry (ICP-MS, Agilent 7500ce, Agilent Technologies, Inc., 71034 Böblingen, Germany). Oxygen containing functional groups on the MWCNT induced by the functionalization procedure were identified using X-ray photoelectron spectroscopy (XPS, Phi 5600, Physical Electronics Inc., Chanhassen, MN 55317, USA).

For preparation of nanoparticle suspensions, 1 mg of ^{14}C -labeled functionalized MWCNT were added to 1 L of 1 mM KCl solution and ultrasonicated for approximately 10 min at 65 W using a cup horn sonicator (Branson Sonifier[®] W-250, Danbury, CT 06813-1961, USA) until no aggregates were visible. To obtain suspensions with lower MWCNT concentrations (0.01 and 0.005 mg L^{-1}), the stock suspensions ($1 \text{ mg MWCNT L}^{-1}$) were diluted with 1 mM KCl to achieve the desired concentrations. The concentration of the MWCNT suspensions was assessed by measuring the radioactivity of five 2.5 ml aliquots.

Each aliquot was added to 5 mL of scintillation cocktail (Insta-Gel Plus, Perkin Elmer, 63110 Rodgau, Germany), shaken, and the radioactivity was measured using a liquid scintillation counter (LSC, Perkin Elmer, 63110 Rodgau, Germany). The standard deviation of the radioactivity measured in the five replicates was low, indicating that the MWCNT suspensions were homogeneous. The specific radioactivity of the functionalized MWCNT was approximately 3.2 MBq mg⁻¹.

The stability and electrophoretic mobility of suspensions were determined using unlabeled functionalized MWCNT. The critical coagulation concentration of 10 mg L⁻¹ MWCNT in KCl (1–100 mM) solution was determined by visual observations over a 24 h period. The hydrodynamic radius and the electrophoretic mobility of MWCNT suspensions (1 mg L⁻¹, 1 mM KCl, pH 8.5) were determined using a Zetasizer Nano (Malvern Instruments GmbH, 71083 Herrenberg, Germany). The hydrodynamic radius of MWCNT was measured immediately after suspension preparation, after 1 h, and after 24 h.

2.2. Porous media

Three quartz sands with different median grain sizes were utilized in the experiments. In particular, we employed two high purity quartz sands (Quarzwirke GmbH, 50226 Frechen, Germany) with an average grain size of 350 µm and 240 µm, and a sterile fused silica sand (Teco-Sil[®], C-E Minerals, King of Prussia, PA, 19406, USA) with an average grain size of 607 µm. The sands were sequentially treated for 2 h with 65% nitric acid to remove metal oxides, and then 10% peroxide to eliminate organic material (Mattison et al., 2011). The organic carbon content of the sands was below 0.01 wt%. The sands were repeatedly rinsed with deionized water following both acid and peroxide treatments until a neutral pH was achieved in the rinse water. Electrophoretic mobilities of milled sand samples were determined in 1 mM KCl solution using the previously described Zetasizer Nano.

2.3. Column transport experiments

Stainless steel columns with an inner diameter of 3 cm and a length of 12 cm were used for all experiments. The column ends were fitted with a stainless steel plate (1 mm openings) and a PTFE mesh (200 µm openings) to support the sand and

to ensure uniform flow. The columns were incrementally filled with porous medium by trickling sand and deionized water into the column, and then tapping the column with a rubber mallet. The packed column was connected to a pump (MCP V 5.10, Ismatec SA, 8152 Glattbrugg, Switzerland) on the inlet side and a fraction collector (Foxy Jr.[®], Teledyne Isco Inc., Lincoln, NE 68504, USA) on the outlet side. A Darcy velocity of 0.62–0.66 cm min⁻¹ (Table 1) was applied for all experiments; equivalent to a pore water velocity of 1.39–1.66 cm min⁻¹. The flow direction was from the column bottom to the top. Preliminary transport studies were conducted using an empty column to determine losses of MWCNT due to the experimental setup. The initial MWCNT concentration (C_0) that was applied to the column was corrected for these losses.

The wet-packed column was rinsed with around 30 pore volumes of the 1 mM KCl solution before starting a transport experiment. A pulse of approximately 3 pore volumes of a conservative tracer (1 mM KBr) was applied to determine the column porosity and dispersivity. Afterwards, this tracer was flushed to background levels using 1 mM KCl solution. Effluent solutions were collected using the fraction collector every 30 s (e.g., 2.3 mL per vial). The effluent bromide concentrations were determined using a high performance liquid chromatograph (STH 585, Dionex, Sunnyvale, CA, USA) equipped with a UV-detector (UV2075, Jasco, Essex, UK).

The same procedure was repeated using the MWCNT suspensions. In this case, the effluent concentrations of MWCNT were measured using the previously discussed liquid scintillation counter method. Retention profiles for MWCNT were also determined after recovery of the breakthrough curves. In this case, the packed column was excavated in 0.5–1 cm thick increments. The sand from each layer was dried and then homogenized using a mill. The crushed sand was then divided into five 500 mg replicates and combusted at 900 °C using a biological oxidizer (OX 500, R.J. Harvey Instrumentation Corporation, Tappan, NY 10983, USA). The emerging ¹⁴CO₂ was dissolved in vials filled with scintillation cocktail (Oxisolv[®], MERCK KGAA, 64293 Darmstadt, Germany) and the radioactivity was measured using the liquid scintillation counter. Table 1 summarizes measured column properties determined from the conservative tracer experiments and mass balance information for MWCNT.

Table 1 – Experimental conditions, hydraulic parameters, and mass balance information (as fractions of the total applied mass; eff – effluent, soil – soil profile) for all column experiments. The electrolyte was 1 mM KCl.

MWCNT input concentration [mg L ⁻¹]	d_c [µm]	q [cm min ⁻¹]	Pore water velocity [cm min ⁻¹]	Porosity	Disp. ^a [cm]	CNT eff ^b	CNT soil ^c	Total mass balance
0.01	240	0.64	1.39	0.46	0.029	0.05	0.91	0.96
0.01	350	0.63	1.66	0.38	0.043	0.27	0.72	0.99
0.01	607	0.62	1.51	0.41	0.090	0.51	0.46	0.98
0.005	350	0.64	1.45	0.44	0.051	0.13	0.95	1.07
1	240	0.64	1.42	0.45	0.038	0.04	0.82	0.85
1	350	0.66	1.53	0.43	0.052	0.33	0.56	0.88
1	607	0.66	1.43	0.46	0.069	0.73	0.21	0.94

a Disp. is the longitudinal dispersivity estimated on basis of the conservative tracer BTC.

b CNT eff is the total amount of CNT in the liquid phase.

c CNT soil is the total amount of CNT in the solid phase.

2.4. Mathematical modeling

Transport experiments were analyzed using the HYDRUS-1D code, a finite element model for simulating one-dimensional movement of water, heat, and multiple solutes in (variably) saturated media (Šimůnek et al., 2008). The code includes a nonlinear least squares optimization routine (Marquardt, 1963) that allows model parameters to be inversely fitted to experimental breakthrough curves (BTC) and retention profiles (RP). Weights to data points were adjusted so that the contributions to the minimized objective function by the sum of squared deviations between measured and fitted values were approximately the same for BTC and RP. The conservative tracer BTC for each column was simulated using the advective dispersive equation (ADE) and the column porosity and dispersivity was obtained by inverse optimization (Table 1).

The transport of MWCNT was simulated using the ADE with terms for one site kinetic retention. The total mass balance equation is written as (Gargiulo et al., 2007):

$$\frac{\partial \theta C}{\partial t} + \rho \frac{\partial S}{\partial t} = \theta D \frac{\partial C}{\partial x} - \frac{\partial q C}{\partial x} \quad (1)$$

where θ [–] is the volumetric water content, ρ is the bulk density of the porous media [ML^{-3} , where M and L denote units of mass and length, respectively], t is the time [T; T denotes units of time], x is the spatial coordinate [L], q is the flow rate [LT^{-1}], C is the particle concentration in the aqueous phase [N_cL^{-3} , where N_c is the number of MWCNT], S is the solid phase particle concentration [N_cM^{-1}], and D is the hydrodynamic dispersion coefficient [L^2T^{-1}]. The corresponding solid phase particle mass balance equation is given as:

$$\rho \frac{\partial S}{\partial t} = \theta k_1 \psi C - k_2 \rho S \quad (2)$$

where k_1 [T^{-1}] is the first-order retention coefficient [T^{-1}], k_2 is the first-order detachment coefficient [T^{-1}], and ψ [–] is a dimensionless function to account for time and depth-dependent retention. The parameter ψ is given as:

$$\psi = \left(1 - \frac{S}{S_{\max}}\right) \left(\frac{d_c + x}{d_c}\right)^{-\beta} \quad (3)$$

where S_{\max} [N_cM^{-1}] is the maximum solid phase particle concentration, d_c [L] is the median diameter of the sand grains, and β [–] is an empirical variable that controls the shape of the retention profile.

The above model formulation is very flexible and can account for time-dependent breakthrough curves and retention profiles that are exponential, uniform, and/or hyper-exponential with depth. The first term on the right side of Eq. (3) accounts for time-dependent blocking/filling of retention sites using a Langmuirian approach (Gargiulo et al., 2007). This blocking term implies that retention decreases with time and that the retention profile becomes uniform with depth as S approaches S_{\max} . The second term on the right side of Eq. (3) describes depth-dependent retention (e.g., a decreasing retention rate with depth). When $\beta = 0$ this term equals 1 and an exponential distribution of retained MWCNT is predicted

with depth similar to conventional filtration theory. Conversely, when $\beta > 0$ is employed then the retention profile of MWCNT exhibits a hyper-exponential shape (e.g., a higher deposition rate close to the column inlet). Bradford et al. (2003) found an optimal value of $\beta = 0.432$ for different sized spherical latex microspheres and sand grains. However, this value of β did not adequately describe the observed depth-dependency in retention profile shape for the non-spherical MWCNT. This parameter was therefore re-estimated by simultaneously fitting β and k_1 to BTC and RP from the three sized sands. Based on this information a value of β for MWCNT was estimated from the average value from these experiments as 0.765 (standard deviation = 0.1). A similar value for β (0.8) was employed by Wang et al. (2012b) in MWCNT transport studies.

Four model formulations based on Eqs. (1)–(3) will be considered in this work. The conventional attachment and detachment model (M1) is obtained by setting $\psi = 1$. A model that includes attachment, detachment, and Langmuirian blocking (M2) is achieved when $\beta = 0$. A depth-dependent retention model (M3) is acquired by setting $\beta = 0.765$ and setting S_{\max} to a large value so that the first term on the right side of Eq. (3) goes to 1. Finally, a time and depth-dependent retention model (M4) is given when $\beta = 0.765$ and S_{\max} is set equal to a value resulting in the first term on the right side of Eq. (3) being smaller than 1.

3. Results and discussion

3.1. Characterization of MWCNT

Results of the ICP-MS measurements indicated that catalyst impurities were significantly removed after the functionalization process. The acid treatment reduced the amount of Mg, Mn, Co, and Al from 3.26 wt% to less than 0.07 wt%. Thus, metal impurities were almost completely removed and were not expected to influence interaction of MWCNT with the porous media.

Fig. 1 shows XPS spectra of as-received and functionalized MWCNT. The intensity of the binding energy of the O 1s spectra (Fig. 1a) was significantly higher after the acid treatment, indicating that functionalization produced an increased amount of groups containing oxygen. The two materials also show differences in their C 1s spectra (Fig. 1b). The peak at 285 eV, representing the sp^2 carbon atoms of the graphene sheets, was dominant for both samples (Xia et al., 2007). Between 287 and 293 eV the spectra of the functionalized MWCNT showed a shoulder that is attributable to carbon atoms exhibiting bonds to oxygen atoms (Xia et al., 2007). Hence, the XPS spectra demonstrate that acid treatment of MWCNT produced functional groups that carried oxygen.

Transmission electron microscope (TEM) images (Fig. 2) show that MWCNT were tortuous particles with a high aspect ratio. At higher magnification, the multiple walls of carbon were visible (Fig. 2b). The size distribution of MWCNT is very heterogeneous. Pauluhn (2010) reported that MWCNT had a median diameter of 10–15 nm and a median length of 200–1000 nm. Qualitative analysis of Fig. 2 yielded similar results. The hydrodynamic radius of MWCNT dispersed in

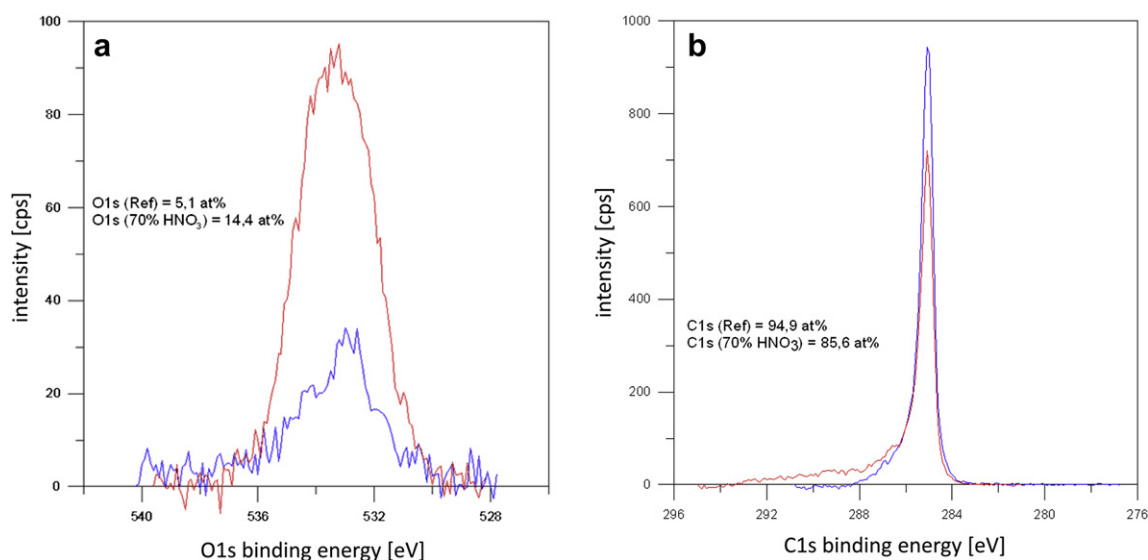


Fig. 1 – High resolution O 1s (a) and C 1s (b) spectra of untreated (blue line) and functionalized (red line) multiwalled carbon nanotubes obtained using X-ray photoelectron spectroscopy.

1 mM KCl was determined using dynamic light scattering (DLS) to range between 170 and 210 nm. DLS measurements and TEM images did not reveal significant changes in size and diameter after the acid treatment.

Reliable determination of MWCNT stability and interaction energies using conventional approaches (DLS and DLVO calculations) is not trivial because of their complex size distribution and configuration (Fig. 2). However, the critical coagulation concentration for unlabeled, functionalized MWCNTs was found to be 40 mM KCl in simple aggregation experiments. The electrolyte concentration used in the transport experiments (1 mM KCl) was significantly below this value. Furthermore, no visual MWCNT aggregates were observed after 4 h in 1 mM KCl solution and the hydrodynamic radius at three measurement times ($t = 0$ h, $t = 1$ h, and $t = 24$ h) was in the same range. Thus, it was assumed that all MWCNT suspensions were stable for the duration of the transport experiments (approximately 1 h). The electrophoretic mobility for MWCNT in 1 mM KCl solution (pH 8.5) was

measured to be $-2.85 \times 10^{-8} \text{ m}^2 \text{ V}^{-1} \text{ s}^{-1}$. The electrophoretic mobility values for the sands were -3.90×10^{-8} (240 μm), -4.47×10^{-8} (350 μm), and $-3.15 \times 10^{-8} \text{ m}^2 \text{ V}^{-1} \text{ s}^{-1}$ (607 μm). The negative charge on both MWCNT and sand, and the low IS conditions, suggests that repulsive electrostatic conditions, that were unfavorable for attachment, existed for MWCNT during the transport experiments.

3.2. Effect of grain size

Column experiments were conducted to assess the effect of the collector grain size on MWCNT transport and retention. Fig. 3 presents observed and simulated BTCs for MWCNT in three different sized sands (240, 350, and 607 μm) when $q = 0.62\text{--}0.66 \text{ cm min}^{-1}$, IS = 1 mM, and $C_0 = 0.01 \text{ mg L}^{-1}$. The BTCs are plotted as the normalized effluent concentration (C/C_0) as a function of pore volumes that have been flushed through the column. The corresponding observed and simulated RPs for the MWCNT are shown in Fig. 4. The RPs are

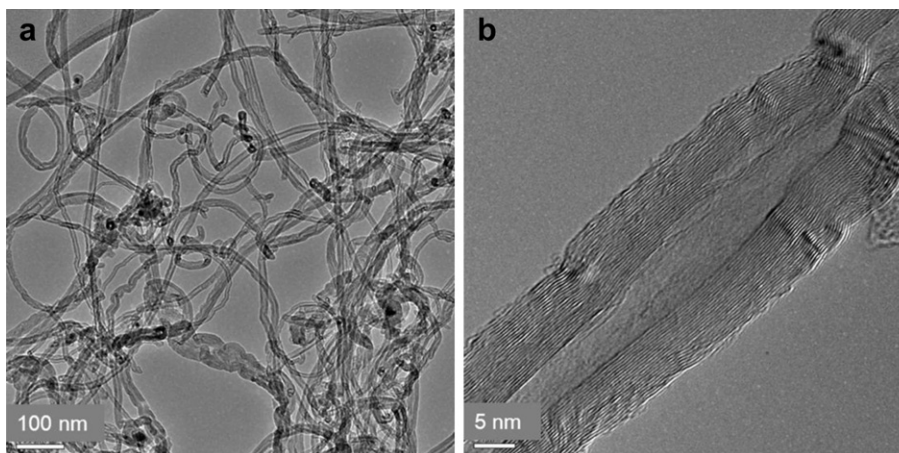


Fig. 2 – Transmission electron micrographs of multiwalled carbon nanotubes at different magnifications.

plotted as normalized solid phase concentration (S/C_0) as a function of distance. The total mass balance information presented in Table 1 ranged from 0.85 to 1.07.

The MWCNT breakthrough curves (Fig. 3) reached the column outlet only slightly after the conservative tracer (data not shown), indicating that size exclusion was negligible for MWCNT (Bradford et al., 2003). A clear decrease in the maximum MWCNT effluent concentration occurred with decreasing grain size. This can partially be explained by an increasing rate of mass transfer to the solid surface with a decrease in sand grain size as predicted by filtration theory (Yao et al., 1971; Tufenkji and Elimelech, 2004). The MWCNT BTCs in the 240 and 350 μm sands also exhibited some time-dependent blocking behavior (increasing breakthrough concentrations with time), suggesting that retention locations were being filled over time. The observed concentration tailing was negligible after recovery of the BTC. The value of k_2 was therefore set equal to zero for all of these simulations.

The fitted model parameters to the BTCs (M1 and M2) as well as to BTCs and RPs (M3 and M4) are provided in Table 2, as well as the Pearson's correlation coefficient for the BTC (R_{eff}^2). A direct comparison between k_1 values for the four model formulations is not meaningful since models M1 and M2 do not account for a depth-dependency, whereas models M3 and M4 do. All four model formulations (M1, M2, M3, and M4) described the MWCNT BTCs quite well with (R_{eff}^2) > 0.85.

Improved agreement with the BTCs was obtained for models that included the Langmuirian blocking term (M2 and M4). The Akaike information criterion (AIC) (Akaike, 1974) was used to assess the relative ability of the four model formulations to describe the BTC and RP data. The AIC value is a measure of the goodness of a fit that penalizes for adding fitting parameters; i.e., the model with the lowest value of AIC is preferred. The AIC decreases from M1 to M4, indicating that M4 provides the best agreement with the observed data. For a particular model, k_1 and S_{max} increased with decreasing grain size. Previous studies on the transport and deposition of fullerene (C_{60}) nanoparticles reported similar trends (Li et al., 2008). These trends reflect an increasing rate of retention and more retention locations in the finer textured sand.

MWCNT retention shown in Fig. 4 was highest close to the column inlet and then rapidly decreased with distance. Consistent with the BTCs shown in Fig. 3, greater MWCNT retention occurred with decreasing sand size. Large deviations were observed between experimental and simulated RPs for models M1 and M2. The Pearson's correlation coefficient for the RP (R_{soil}^2) was less than 0.58. Models M1 and M2 tended to underestimate the high concentrations near the column inlet and overestimated the concentrations at greater distances, especially for finer textured sand. Thus, RPs were not considered for fitting model parameters using models M1 and M2. These observations indicate that the experimental RPs

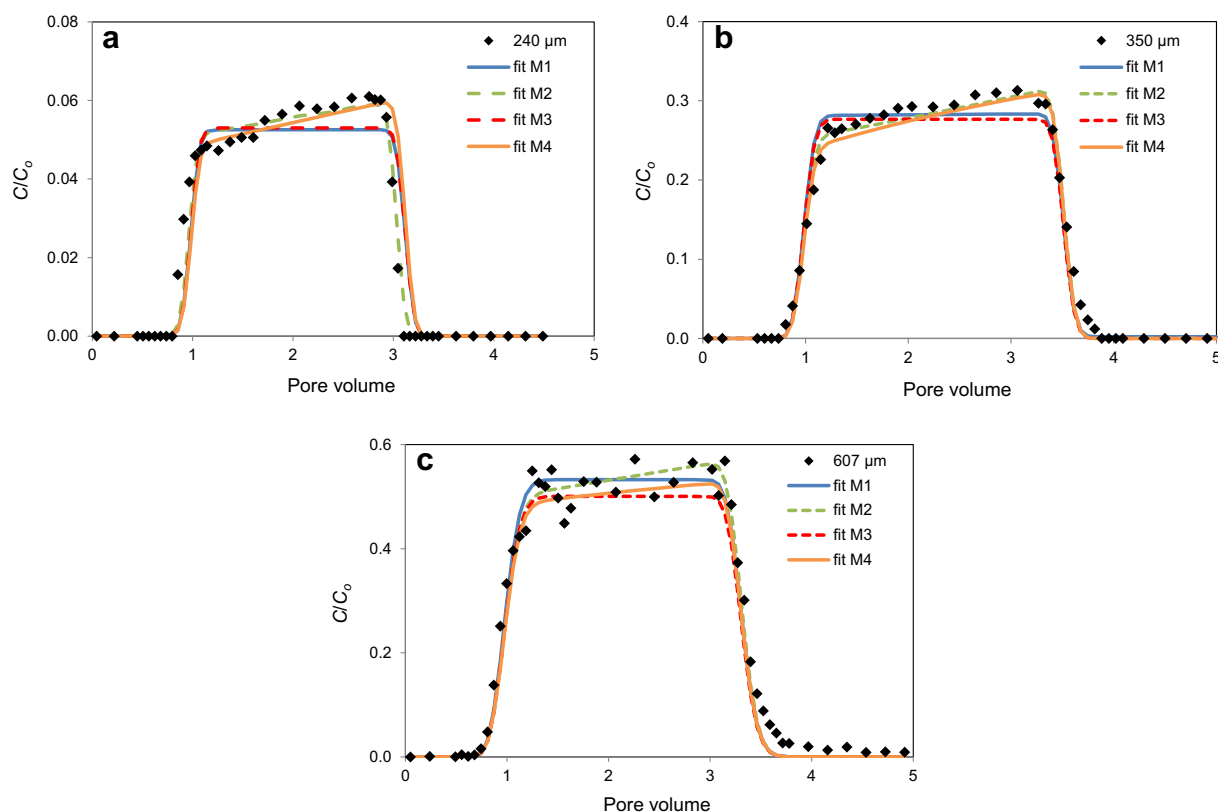


Fig. 3 – Observed and simulated breakthrough curves for MWCNT in three different sized quartz sands: 240 μm (a), 350 μm (b), and 607 μm (c). Experimental data were fitted with four different models including: attachment and detachment (M1); attachment, detachment, and blocking (M2); depth-dependent retention (M3); and blocking combined with depth-dependent retention (M4). The flow rate was 0.62–0.66 cm min^{-1} , the electrolyte was 1 mM KCl, and the MWCNT input concentration was 0.01 mg L^{-1} . Note different vertical scales in the figures.

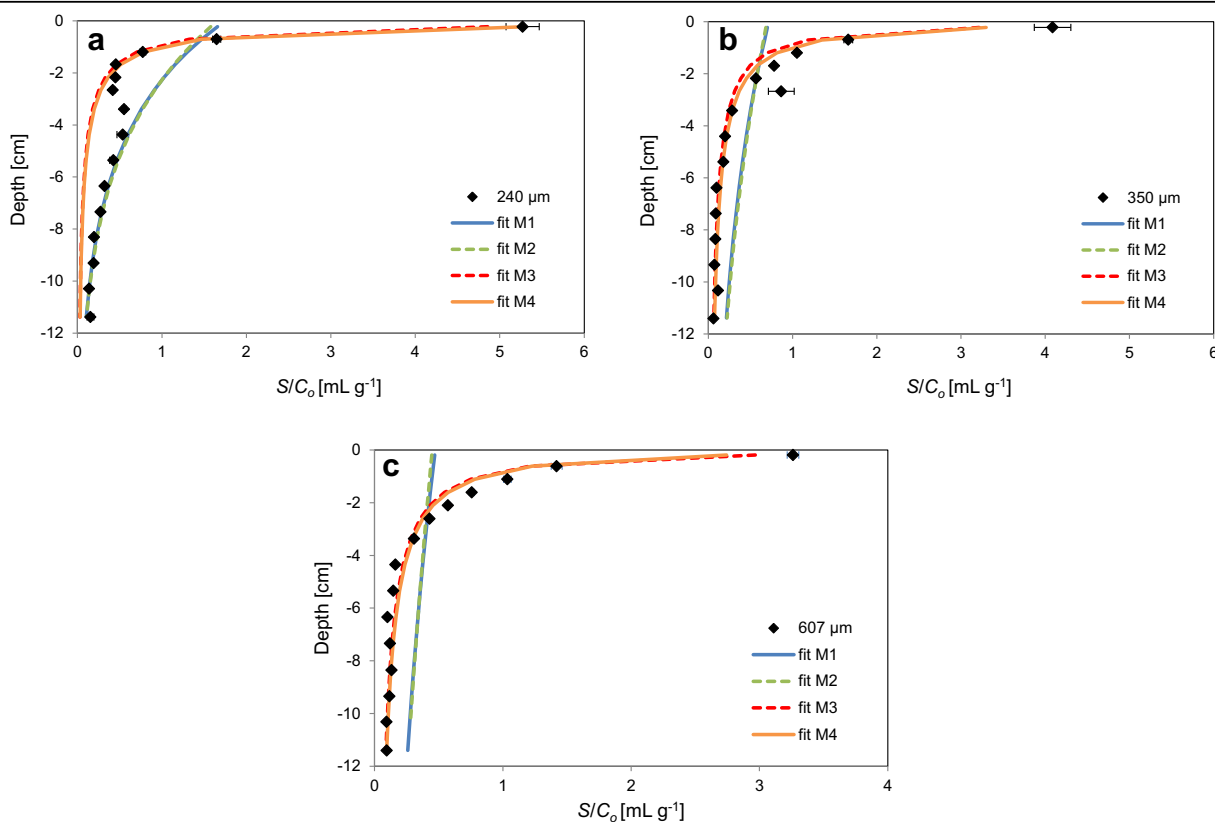


Fig. 4 – Observed and simulated retention profiles for MWCNT in three different sized quartz sands: 240 μm (a), 350 μm (b), and 607 μm (c). Experimental data were simulated with four different models including: attachment and detachment (M1); attachment, detachment, and blocking (M2); depth-dependent retention (M3); and blocking combined with depth-dependent retention (M4). The flow rate was 0.62–0.66 cm min^{-1} , the electrolyte was 1 mM KCl, and the MWCNT input concentration was 0.01 mg L^{-1} .

were hyper-exponential with distance, and that the retention coefficient exhibited a depth-dependency. Models M3 and M4 include a depth-dependency in the retention coefficient, and therefore provided a much better description of the MWCNT RPs than either M1 or M2. The value of (R_{soil}^2) for the M3 and M4 models was >0.98 . Model M4 provided the best overall description of the data when both BTCs and RPs were considered.

Hyper-exponential RPs have frequently been reported in the literature for colloids, microorganisms, and nanoparticles under unfavorable attachment conditions (Bradford and Bettahar, 2006; Bradford and Toride, 2007; Gargiulo et al., 2007, 2008; Wang et al., 2011; Wang et al., 2012a). A variety of reasons for hyper-exponential RPs have been identified, including: straining at grain–grain contacts and surface roughness locations (Shellenberger and Logan, 2001; Bradford et al., 2002, 2003; Yoon et al., 2006), particle aggregation (Chen and Elimelech, 2006, 2007; Chatterjee and Gupta, 2009; Chatterjee et al., 2010), hydrodynamic factors (Li et al., 2005; Bradford et al., 2009; Wang et al., 2011), and chemical heterogeneity on the sand and colloid (Bolster et al., 1999; Li et al., 2004; Tufenkji and Elimelech, 2005; Tong and Johnson, 2006). The relative contribution of each of these factors to the observed RP data is difficult to ascertain without additional information. However, our data does clearly indicate a strong dependency of the RP shape on the grain size under

low IS conditions. The contribution of physical processes to the observed hyper-exponential RPs has to be proven. However, other results in the literature indicate that straining played a dominant role in the CNT retention under low IS conditions (Jaisi et al., 2008; Wang et al., 2012b).

Previous transport studies with CNT measured and simulated only BTCs (Jaisi et al., 2008; Jaisi and Elimelech, 2009; Liu et al., 2009; Mattison et al., 2011). Determination and modeling of retention profile are scarce (Wang et al., 2012b). Accurate simulation of both BTCs and RPs is needed in order to assess the fate and risks associated with MWCNT migration. To illustrate this point, Fig. 5 presents the simulated RPs of MWCNT in the three different sized sands over a distance of 500 cm when using the various model formulations that were calibrated to the column BTC (M1 and M2) or BTC and RP (M3 and M4) data, respectively (Fig. 3). In Fig. 5 and the discussion below we set the lower limit of the predicted S/C_0 to $1\text{E}-5 \text{ mL g}^{-1}$. Increasing deviations in the model predictions occurred with transport distance and grain size. The M1 and M2 predictions were quite similar for a given grain size, with no breakthrough at a depth of 500 cm. The maximum transport distance predicted by the M1 and M2 models was around 200 cm in the coarsest textured 607 μm sand. In contrast, models M3 and M4 predict similar low levels of MWCNT breakthrough at 500 cm for the two largest grain sizes (350 and 607 μm). Consequently, using M1 and M2 to predict MWCNT

Table 2 – Fitted model parameters using different model formulations. Correlation of observed and fitted data is reflected by $R_{\text{eff+soil}}^2$ for BTC and RP, by R_{eff}^2 for BTC, and by R_{soil}^2 for RP.

C_o [mg L ⁻¹]	d_c [μm]	Model	$R_{\text{eff+soil}}^2$	R_{eff}^2	R_{soil}^2	β	k_1 [min ⁻¹]	Standard error k_1	k_2 [min ⁻¹]	Standard error k_2	S_{max} [Bq g ⁻¹]	Standard error S_{max}
0.01	240	M1	0.57	0.88	0.44		0.34	0.47E+1				
0.01	350	M1	0.45	0.98	0.53		0.17	1.75E-1				
0.01	607	M1	0.32	0.98	0.49		0.08	2.90E-1				
0.01	240	M2	0.54	0.96	0.54		0.35	0.43E+1			289	0.15
0.01	350	M2	0.43	0.99	0.50		0.19	0.24E+1			68	5.40
0.01	607	M2	0.30	0.98	0.47		0.09	0.34E-2			49	14.40
0.01	240	M3	0.98	0.86	0.99	0.765	11.47	0.25E-2				
0.01	350	M3	0.96	0.98	0.99	0.765	4.70	0.47E+1				
0.01	607	M3	0.99	0.98	0.99	0.765	1.64	0.43E-1				
0.01	240	M4	0.98	0.91	0.99	0.765	11.97	2.37E-1			2760	717
0.01	350	M4	0.98	0.99	0.99	0.765	5.14	0.69E-1			338	45
0.01	607	M4	0.98	0.98	1.00	0.765	1.72	0.57E-1			303	129
0.01	240	M4	0.98	0.74	0.99	0.765	11.75	2.52E-3			11,967	NF
0.01	350	M4	0.97	0.95	0.98	0.765	4.73	1.22E-1			4659	NF
0.01	607	M4	0.98	0.97	0.99	0.765	1.60	0.57E-1			1516	NF
1	240	M4	0.95	0.98	0.93	0.765	22.94	4.26E-1	0.5E-3	NF	11,967	1419
1	350	M4	0.97	0.98	0.97	0.765	7.27	2.64E-1	0.3E-2	0.17E-2	4659	283
1	607	M4	0.98	0.97	0.81	0.765	1.69	1.09E-1	0.3E-2	0.22E-2	1516	129
00.005	350	M4	0.97	0.78	0.98	0.765	6.75	3.61E-1			4659	NF

NF – denotes not fitted.

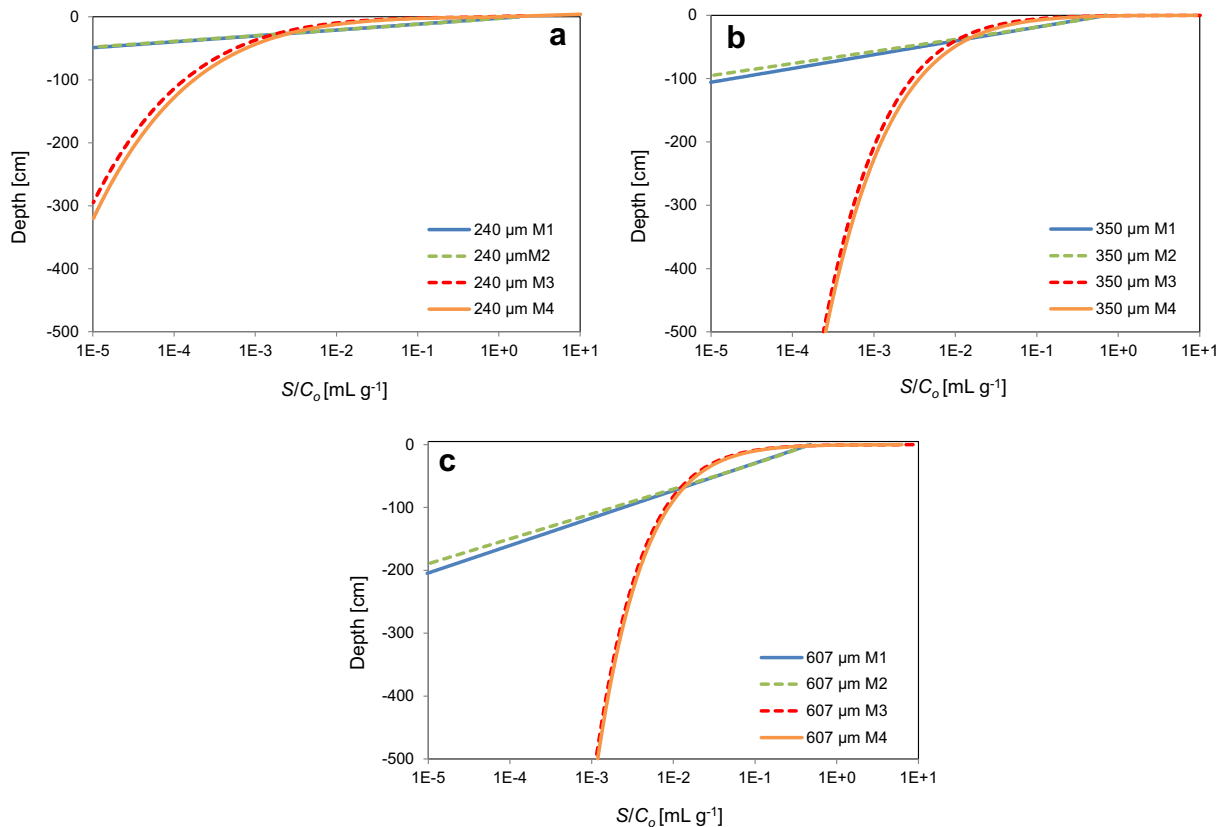


Fig. 5 – Predicted retention profiles for MWCNT in 500 cm long columns packed with 240 μm (a), 350 μm (b), and 607 μm (c) sand. Here the normalized solid phase concentration (S/C_o) is plotted on a log-scale as a function of distance. Simulations employed model parameters determined in Figs. 3 and 4. Four different model formulations were considered, namely: attachment and detachment (M1); attachment, detachment, and blocking (M2); depth-dependent retention (M3); and blocking combined with depth-dependent retention (M4).

fate would lead to the conclusion that MWCNT will be retained in the various sands before reaching a depth of around 200 cm. In contrast, M3 and M4 would predict a transport of MWCNT to depths greater than 500 cm. Since models M3 and M4 provided the best description of the BTCs and RPs at the column scale (Figs. 3 and 4), the predictions of these models are more reliable than the predictions obtained from the other two models (M1 and M2).

3.3. Effect of MWCNT input concentration

Additional column experiments were performed to investigate the influence of MWCNT input concentrations. Fig. 6 presents observed and simulated BTCs (Fig. 6a) and RPs (Fig. 6b) for MWCNT in 350 μm sand when $q = 0.62\text{--}0.66\text{ cm min}^{-1}$, $IS = 1\text{ mM}$, and $C_o = 1, 0.01,$ and 0.005 mg L^{-1} . Based on the findings of the previous section, only simulation results from model M4 were considered in Fig. 6. Simulation fits to BTCs and RPs were very good, with a $(R_{\text{eff}}^2) > 0.97$ and $(R_{\text{soil}}^2) > 0.96$. Tables 1 and 2 provide a summary of the associated experimental, mass balance, and model parameters.

Inspection of Fig. 6a indicates that the fraction of the injected mass of MWCNT that was recovered in the effluent increased with C_o . In addition, the shape of the BTC was much steeper for the highest $C_o = 1\text{ mg L}^{-1}$ condition. These trends may be explained by blocking behavior as retention locations fill up over time and produce increasing effluent concentrations (Bradford and Bettahar, 2006). Consistent with observations in Fig. 6a, a higher C_o is expected to fill a given S_{max} more rapidly. The value of S_{max} was fitted for the highest C_o and then kept constant for the lower input concentrations. The fitted retention rate parameter k_1 was similar for all C_o . After recovery of the BTC, concentration tailing tended to be low, but was most pronounced for the highest $C_o = 1\text{ mg L}^{-1}$ condition. This indicates that some of the MWCNT retention was reversible at higher C_o when S_{max} was filled to a greater extent (Kretzschmar et al., 1995).

Similar to the BTCs (Fig. 6a), the shape of the RPs was also sensitive to C_o (Fig. 6b). In particular, the fraction of MWCNT

retained close to the column inlet increased with decreasing C_o . Conversely, the RPs became less hyper-exponential (more uniform) with increasing C_o . Blocking provides an explanation for changes in the RPs shape with C_o (Bradford and Bettahar, 2006; Bradford et al., 2009; Zhang et al., 2010; Kim et al., 2011). As MWCNT retention approaches S_{max} the overall rate of retention decreases and the RPs become uniform with depth (Bradford et al., 2009).

Results from Fig. 6 demonstrate that C_o can have a large impact on the transport and retention behavior of MWCNT. Enhanced retention and limited mobility of MWCNTs is expected for lower, more environmentally relevant concentrations of MWCNT. These C_o effects need to be considered in models that are used to predict MWCNT fate and risks, otherwise they may overestimate their transport potential and groundwater concentrations.

3.4. Effect of grain size and MWCNT input concentration

Fig. 7 presents observed and simulated BTCs (Fig. 7a) and RPs (Fig. 7b) for MWCNT in three different sized sands (240, 350, and 607 μm) when $q = 0.62\text{--}0.66\text{ cm min}^{-1}$, $IS = 1\text{ mM}$, and $C_o = 1.0\text{ mg L}^{-1}$. Simulation results from model M4 were considered in Fig. 7. Simulation fits to BTCs and RPs were good, with a $(R_{\text{eff}}^2) > 0.97$ and $(R_{\text{soil}}^2) > 0.81$. Tables 1 and 2 provide a summary of the associated experimental, mass balance, and model parameters. Similar to Figs. 3 and 4, Fig. 7 examines the influence of grain size on MWCNT transport and retention. However, the experiments shown in Fig. 7 were conducted at a C_o that was two orders of magnitude higher than in Figs. 3 and 4.

Comparison of Figs. 3 and 4 and 7 reveals a similar trend of increasing MWCNT retention (decreasing breakthrough) with decreasing grain size at both C_o levels. In contrast, the time-dependent blocking behavior shown in the BTCs (e.g., increase in the normalized effluent concentrations shown in Figs. 3 and 7a) was much steeper for experiments conducted at the higher C_o . The RPs were also more hyper-exponential at the lower C_o (see Figs. 4 and 7b). As explained in the last section, these trends occur because retention locations were

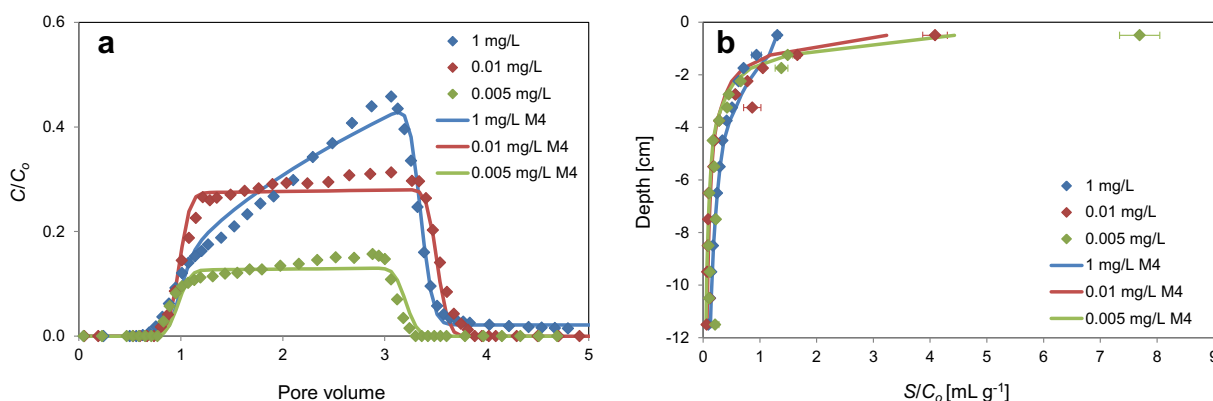


Fig. 6 – Observed and simulated breakthrough curves (a) and retention profiles (b) for MWCNT at input concentrations (C_o) equal to 1, 0.01, and 0.005 mg L^{-1} . The flow rate was $0.62\text{--}0.66\text{ cm min}^{-1}$, the electrolyte was 1 mM KCl, and the grain size of the quartz sand was 350 μm . The data was simulated using a model combining depth- and time-dependent retention (M4).

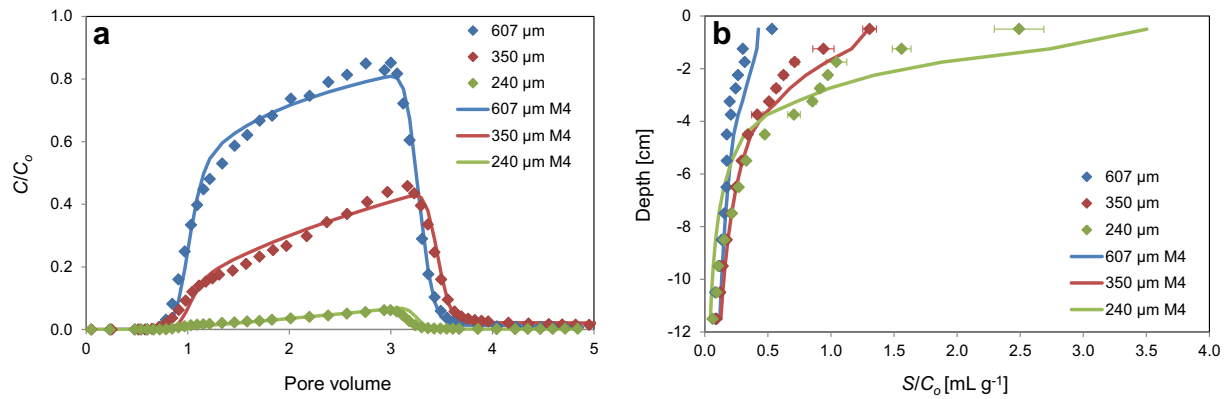


Fig. 7 – Observed and simulated breakthrough curves (a) and retention profiles (b) for MWCNT in three different sized quartz sands: 240 μm (a), 350 μm (b), and 607 μm (c). The flow rate was 0.62–0.66 cm min⁻¹, the electrolyte was 1 mM KCl, and the MWCNT input concentration was 1 mg L⁻¹. The data was simulated using a model combining depth- and time-dependent retention (M4).

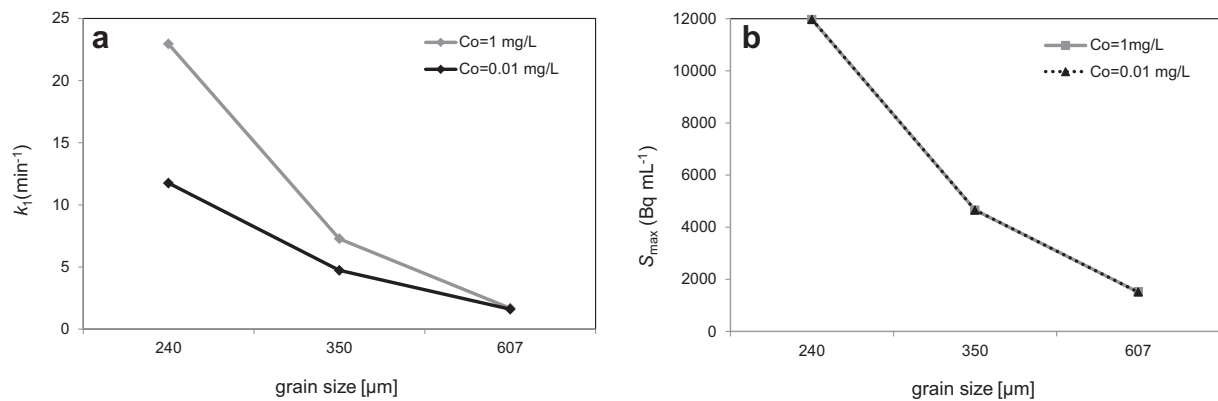


Fig. 8 – Plots of the depth-dependent (model M4) retention coefficient (k_1) (a) and the maximum solid phase particle concentration (S_{max}) (b) as a function of sand grain size for input MWCNT concentrations (C_0) of 1 and 0.01 mg L⁻¹.

filled more rapidly at a higher C_0 . However, close inspection of Figs. 3, 4 and 7 indicates that this concentration-dependent transport behavior was also a function of the sand grain size.

Examination of parameters k_1 (Fig. 8a) and S_{max} (Fig. 8b) as a function of grain size for the two C_0 levels revealed that the values of k_1 and S_{max} both increased with decreasing grain size. As mentioned above, this reflects greater MWCNT retention rates and number of retention locations in the finer textured sand. However, higher C_0 values accentuated this trend with k_1 and this rate of enhancement increased with decreasing grain size. Hence, the observed concentration dependency of MWCNT transport became more important with increasing C_0 and decreasing grain size. In contrast to our observations with MWCNT, Bradford and Bettahar (2006) observed for spherical latex microspheres that concentration-dependent colloid transport behavior became more important with increasing grain size. These trends can be explained by the effect of porous media's pore structure on MWCNT retention (Tan et al., 1994). The non-spherical MWCNT have a high aspect ratio and we hypothesize that solid phase MWCNT may create a porous network with the ability to retain particles (Sumanasekera et al., 2010; Xin et al.,

2012). It is logical to anticipate that the retained MWCNT network will become more significant at higher C_0 and in smaller grain sized sand. This finding suggests that the particle shape will have a strong influence on concentration-dependent colloid transport.

4. Conclusions

This study highlights the importance of considering input concentration and retention profiles to allow reliable predictions of MWCNT transport and fate. The work provides new information on the mobility of multi-walled carbon nanotubes because both breakthrough curves and retention profiles were considered. Additionally, experiments were performed using more environmentally relevant MWCNT concentrations. Results demonstrate that normalized MWCNT transport increased with higher input concentrations and in coarser textured sand. The retention profiles showed that the majority of MWCNT retention occurred near the surface of the porous medium, especially for lower input concentrations and smaller sand sizes. Simulations that considered a combination of time-

and depth-dependent retention provided a good description of the experimental data. Analysis of model parameters demonstrated that concentration dependent transport behavior became more important for smaller grain sizes and higher input concentrations. These trends were attributed to the complex shape and deposition morphology of MWCNT in smaller pore spaces at higher input concentrations. The results of this study suggest that functionalized MWCNT tend to be mobile in sandy subsurface environments, and may be transported to depths greater than 500 cm. Thus, aquifer contamination cannot be excluded. Further work is needed to assess the mobility of MWCNT in natural porous media, such as undisturbed soils.

Acknowledgements

This research was performed within the framework of the 'NanoFlow'-project supported by the German Federal Ministry of Education and Research. Analysis of bromide in the liquid samples by Stephan Köppchen is highly appreciated. The technical assistance of Herbert Philipp is gratefully acknowledged. We also thank Wolfgang Schierenberg for the determination of the critical coagulation concentration.

REFERENCES

- Akaike, H., 1974. A new look at the statistical model identification. *Automatic Control, IEEE Transactions on* 19 (6), 716–723.
- Bierdel, M., Buchholz, S., Michele, V., Mleczko, L., Rudolf, R., Voetz, M., Wolf, A., 2007. Industrial production of multiwalled carbon nanotubes. *Physica Status Solidi (B)* 244 (11), 3939–3943.
- Bolster, C.H., Mills, A.L., Hornberger, G.M., Herman, J.S., 1999. Spatial distribution of deposited bacteria following miscible displacement experiments in intact cores. *Water Resources Research* 35 (6), 1797–1807.
- Bradford, S.A., Bettahar, M., 2005. Straining, attachment, and detachment of oocysts in saturated porous media. *Journal of Environmental Quality* 34 (2), 469–478.
- Bradford, S.A., Bettahar, M., 2006. Concentration dependent transport of colloids in saturated porous media. *Journal of Contaminant Hydrology* 82 (1–2), 99–117.
- Bradford, S.A., Toride, N., 2007. A Stochastic Model for colloid transport and deposition all rights reserved. No part of this periodical may be reproduced or transmitted in any form or by any means, electronic or mechanical, including photocopying, recording, or any information storage and retrieval system, without permission in writing from the publisher. *Journal of Environmental Quality* 36 (5), 1346–1356.
- Bradford, S.A., Yates, S.R., Bettahar, M., Simunek, J., 2002. Physical factors affecting the transport and fate of colloids in saturated porous media. *Water Resources Research* 38 (12), 12.
- Bradford, S.A., Simunek, J., Bettahar, M., van Genuchten, M.T., Yates, S.R., 2003. Modeling colloid attachment, straining, and exclusion in saturated porous media. *Environmental Science & Technology* 37 (10), 2242–2250.
- Bradford, S.A., Kim, H.N., Haznedaroglu, B.Z., Torkzaban, S., Walker, S.L., 2009. Coupled factors influencing concentration-dependent colloid transport and retention in saturated porous media. *Environmental Science & Technology* 43 (18), 6996–7002.
- Chatterjee, J., Gupta, S.K., 2009. An agglomeration-based model for colloid filtration. *Environmental Science & Technology* 43 (10), 3694–3699.
- Chatterjee, J., Abdulkareem, S., Gupta, S.K., 2010. Estimation of colloidal deposition from heterogeneous populations. *Water Research* 44 (11), 3365–3374.
- Chen, K.L., Elimelech, M., 2006. Aggregation and deposition kinetics of fullerene (C₆₀) nanoparticles. *Langmuir* 22 (26), 10994.
- Chen, K.L., Elimelech, M., 2007. Influence of humic acid on the aggregation kinetics of fullerene (C₆₀) nanoparticles in monovalent and divalent electrolyte solutions. *Journal of Colloid & Interface Science* 309 (1), 126–134.
- Farré, M., Gajda-Schranz, K., Kantiani, L., Barceló, D., 2009. Ecotoxicity and analysis of nanomaterials in the aquatic environment. *Analytical and Bioanalytical Chemistry* 393 (1), 81–95.
- Gargiulo, G., Bradford, S., Šimunek, J., Ustohal, P., Vereecken, H., Klumpp, E., 2007. Bacteria transport and deposition under unsaturated conditions: the role of the matrix grain size and the bacteria surface protein. *Journal of Contaminant Hydrology* 92 (3–4), 255–273.
- Gargiulo, G., Bradford, S.A., Simunek, J., Ustohal, P., Vereecken, H., Klumpp, E., 2008. Bacteria transport and deposition under unsaturated flow conditions: the role of water content and bacteria surface hydrophobicity. *Vadose Zone Journal* 7 (2), 406–419.
- Gottschalk, F., Sonderer, T., Scholz, R.W., Nowack, B., 2009. Modeled environmental concentrations of engineered nanomaterials (TiO₂, ZnO, Ag, CNT, fullerenes) for different regions. *Environmental Science & Technology* 43 (24), 9216–9222.
- Handy, R., von der Kammer, F., Lead, J., Hassellöv, M., Owen, R., Crane, M., 2008. The ecotoxicology and chemistry of manufactured nanoparticles. *Ecotoxicology* 17 (4), 287–314.
- Iijima, S., 1991. Helical microtubules of graphitic carbon. *Nature* 354 (6348), 56–58.
- Jaisi, D.P., Elimelech, M., 2009. Single-walled carbon nanotubes exhibit limited transport in soil columns. *Environmental Science & Technology* 43 (24), 9161–9166.
- Jaisi, D.P., Saleh, N.B., Blake, R.E., Elimelech, M., 2008. Transport of single-walled carbon nanotubes in porous media: filtration mechanisms and reversibility. *Environmental Science & Technology* 42 (22), 8317–8323.
- Kim, H., Lee, M., Chae, W., Ezeh, T.D., Walker, S.L., 2011. Coupled effect of input concentration and solution ionic strength on colloid transport in saturated porous media. *International Proceedings of Chemical, Biological, and Environmental Engineering* 17, 195–198.
- Klaine, S.J., Alvarez, P.J.J., Batley, G.E., Fernandes, T.F., Handy, R.D., Lyon, D.Y., Mahendra, S., McLaughlin, M.J., Lead, J.R., 2008. Nanomaterials in the environment: behavior, fate, bioavailability, and effects. *Environmental Toxicology and Chemistry* 27 (9), 1825–1851.
- Köhler, A.R., Som, C., Helland, A., Gottschalk, F., 2008. Studying the potential release of carbon nanotubes throughout the application life cycle. *Journal of Cleaner Production* 16 (8–9), 927–937.
- Kretzschmar, R., Robarge, W.P., Amoozegar, A., 1995. Influence of natural organic matter on colloid transport through saprolite. *Water Resources Research* 31 (3), 435–445.
- Lam, C.W., James, J.T., McCluskey, R., Hunter, R.L., 2004. Pulmonary toxicity of single-wall carbon nanotubes in mice 7 and 90 days after intratracheal instillation. *Toxicological Sciences* 77 (1), 126–134.
- Lam, C.-W., James, J.T., McCluskey, R., Arepalli, S., Hunter, R.L., 2006. A review of carbon nanotube toxicity and assessment of

- potential occupational and environmental health risks. *Critical Reviews in Toxicology* 36 (3), 189–217.
- Li, X., Scheibe, T.D., Johnson, W.P., 2004. Apparent decreases in colloid deposition rate coefficients with distance of transport under unfavorable deposition conditions: a general phenomenon. *Environmental Science & Technology* 38 (21), 5616–5625.
- Li, X., Zhang, P., Lin, C.L., Johnson, W.P., 2005. Role of hydrodynamic drag on microsphere deposition and re-entrainment in porous media under unfavorable conditions. *Environmental Science & Technology* 39 (11), 4012–4020.
- Li, Y., Wang, Y., Pennell, K.D., Abriola, L.M., 2008. Investigation of the transport and deposition of fullerene (C₆₀) nanoparticles in quartz sands under varying flow conditions. *Environmental Science & Technology* 42 (19), 7174–7180.
- Liu, X., O'Carroll, D.M., Petersen, E.J., Huang, Q., Anderson, C.L., 2009. Mobility of multiwalled carbon nanotubes in porous media. *Environmental Science & Technology* 43 (21), 8153–8158.
- Marquardt, D., 1963. An algorithm for least-squares estimation of nonlinear parameters. *Journal of the Society for Industrial and Applied Mathematics* 11 (2), 431–441.
- Mattison, N.T., O'Carroll, D.M., Kerry Rowe, R., Petersen, E.J., 2011. Impact of porous media grain size on the transport of multi-walled carbon nanotubes. *Environmental Science & Technology* 45 (22), 9765–9775.
- Mauter, M.S., Elimelech, M., 2008. Environmental applications of carbon-based nanomaterials. *Environmental Science & Technology* 42 (16), 5843–5859.
- Mueller, N.C., Nowack, B., 2008. Exposure modeling of engineered nanoparticles in the environment. *Environmental Science & Technology* 42 (12), 4447–4453.
- Nagasawa, S., Yudasaka, M., Hirahara, K., Ichihashi, T., Iijima, S., 2000. Effect of oxidation on single-wall carbon nanotubes. *Chemical Physics Letters* 328 (4–6), 374–380.
- Nowack, B., Bucheli, T.D., 2007. Occurrence, behavior and effects of nanoparticles in the environment. *Environmental Pollution* 150 (1), 5–22.
- Pauluhn, J., 2010. Multi-walled carbon nanotubes (Baytubes): approach for derivation of occupational exposure limit. *Regulatory Toxicology and Pharmacology: RTP* 57 (1), 78–89.
- Pumera, M., 2007. Carbon nanotubes contain residual metal catalyst nanoparticles even after washing with nitric acid at elevated temperature because these metal nanoparticles are sheathed by several graphene sheets. *Langmuir* 23 (11), 6453–6458.
- Saleh, N.B., Pfefferle, L.D., Elimelech, M., 2008. Aggregation kinetics of multiwalled carbon nanotubes in aquatic systems: measurements and environmental implications. *Environmental Science & Technology* 42 (21), 7963–7969.
- Shellenberger, K., Logan, B.E., 2001. Effect of molecular scale roughness of glass beads on colloidal and bacterial deposition. *Environmental Science & Technology* 36 (2), 184–189.
- Sinnott, S.B., 2002. Chemical functionalization of carbon nanotubes. *Journal of Nanoscience and Nanotechnology* 2 (2), 113–123.
- Simunek, J., van Genuchten, M.T., Šejna, M., 2008. Development and applications of the HYDRUS and STANMOD software packages and related codes. *Vadose Zone Journal* 7 (2), 587–600.
- Smith, B., Wepasnick, K., Schrote, K.E., Cho, H.-H., Ball, W.P., Fairbrother, D.H., 2009. Influence of surface oxides on the colloidal stability of multi-walled carbon nanotubes: a structure-property relationship. *Langmuir* 25 (17), 9767–9776.
- Sumanasekera, G.U., Chen, G., Takai, K., Joly, J., Kobayashi, N., Enoki, T., Eklund, P.C., 2010. Charge transfer and weak chemisorption of oxygen molecules in nanoporous carbon consisting of a disordered network of nanographene sheets. *Journal of Physics: Condensed Matter* 22 (33), 334208.
- Tan, Y., Gannon, J.T., Baveye, P., Alexander, M., 1994. Transport of bacteria in an aquifer sand: experiments and model simulations. *Water Resources Research* 30 (12), 3243–3252.
- Tian, Y., Gao, B., Silvera-Batista, C., Ziegler, K., 2010. Transport of engineered nanoparticles in saturated porous media. *Journal of Nanoparticle Research* 12 (7), 2371–2380.
- Tian, Y., Gao, B., Wang, Y., Morales, V.L., Carpena, R.M., Huang, Q., Yang, L., 2012. Deposition and transport of functionalized carbon nanotubes in water-saturated sand columns. *Journal of Hazardous Materials* 213–214 (0), 265–272.
- Tong, M., Johnson, W.P., 2006. Colloid population heterogeneity drives hyperexponential deviation from classic filtration theory. *Environmental Science & Technology* 41 (2), 493–499.
- Tufenkji, N., Elimelech, M., 2004. Deviation from the classical colloid filtration theory in the presence of repulsive DLVO interactions. *Langmuir* 20 (25), 10818–10828.
- Tufenkji, N., Elimelech, M., 2005. Spatial distributions of cryptosporidium oocysts in porous media: evidence for dual mode deposition. *Environmental Science & Technology* 39 (10), 3620–3629.
- Wang, D., Paradelo, M., Bradford, S.A., Peijnenburg, W.J.G.M., Chu, L., Zhou, D., 2011. Facilitated transport of Cu with hydroxyapatite nanoparticles in saturated sand: effects of solution ionic strength and composition. *Water Research* 45 (18), 5905–5915.
- Wang, D., Bradford, S.A., Harvey, R.W., Hao, X., Zhou, D., 2012a. Transport of ARS-labeled hydroxyapatite nanoparticles in saturated granular media is influenced by surface charge variability even in the presence of humic acid. *Journal of Hazardous Materials* 229–230 (0), 170–176.
- Wang, Y., Kim, J.H., Baek, J.B., Miller, G.W., Pennell, K.D., 2012b. Transport behavior of functionalized multi-wall carbon nanotubes in water-saturated quartz sand as a function of tube length. *Water Research* 46 (14), 4521–4531.
- Xia, W., Wang, Y., Bergsträsser, R., Kundu, S., Muhler, M., 2007. Surface characterization of oxygen-functionalized multi-walled carbon nanotubes by high-resolution X-ray photoelectron spectroscopy and temperature-programmed desorption. *Applied Surface Science* 254 (1), 247–250.
- Xin, S., Guo, Y.-G., Wan, L.-J., 2012. Nanocarbon networks for advanced rechargeable lithium batteries. *Accounts of Chemical Research* 45 (10), 1759–1769.
- Yao, K.M., Habibian, M.T., O'Melia, C.R., 1971. Water and waste water filtration. concepts and applications. *Environmental Science & Technology* 5 (11), 1105–1112.
- Yoon, J.S., Germaine, J.T., Culligan, P.J., 2006. Visualization of particle behavior within a porous medium: mechanisms for particle filtration and retardation during downward transport. *Water Resources Research* 42 (6), W06417.
- Zhang, W., Morales, V.N.L., Cakmak, M.E., Salvucci, A.E., Geohring, L.D., Hay, A.G., Parlange, J.Y., Steenhuis, T.S., 2010. Colloid transport and retention in unsaturated porous media: effect of colloid input concentration. *Environmental Science & Technology* 44 (13), 4965–4972.